Available online at www.sciencedirect.com

ScienceDirect

Underground Space 8 (2023) 61–79

www.keaipublishing.com/undsp

Experimental and numerical studies of the blast-induced overbreak and underbreak in underground roadways

Zhixian Hong [a], Ming Tao [a,*], Xuejiao Cui [a], Chengqing Wu [b], Mingsheng Zhao [c]

[a] School of Resources and Safety Engineering, Central South University, Changsha, Hunan 410083, China
[b] School of Civil and Environmental Engineering, the University of Technology Sydney, Sydney, NSW 2007, Australia
[c] Poly Xinlian Blasting Engineering Group Co., Ltd., Guiyang, Guizhou 550002, China

Received 20 December 2021; received in revised form 8 March 2022; accepted 17 April 2022
Available online 22 August 2022

Abstract

Overbreak and underbreak are the crucial problems during the blasting excavation of underground tunnels owing to their effects on the construction costs and operational safety. A critical challenge facing overbreak and underbreak control is the difficulty in developing guidelines with respect to various and complex engineering conditions. In this study, a series of field measurements of overbreak and underbreak using the Focus^S 150 laser scanner were performed in a deep roadway of the Kaiyang phosphate mine, China. The distribution and extent of the overbreak and underbreak surrounding the roadway contour were accurately analyzed in accordance with the collected point cloud data. Subsequently, a simplified three-dimensional model was established to simulate the blasting excavation of pre-stressed roadway using the explicit dynamic analysis code LS-DYNA. A comparison of numerical and measurement results revealed that the proposed model was a reliable tool to simulate the overbreak and underbreak induced by blasting excavation. Thereafter, the influences of uncontrollable geological factors such as in situ stress conditions and controllable blasting factors including contour hole spacing (S), charge concentration (β) and decoupled coefficient (ζ) as well as stemming were further numerically investigated. The simulation results indicated that the lateral pressure coefficient significantly affected the distribution pattern of the overbreak and underbreak, while the stress magnitude contributed to their extents. Moreover, a comparison of the simulation findings and the field measurement data indicated that the minimal extents of the overbreak and underbreak corresponding the optimal contour blasting results were obtained at $S = 0.70$ m, $\beta = 0.9$ kg/m and $\zeta = 2.5$, respectively. Furthermore, the contour blastholes stemmed with sand created smaller damage to the periphery rock mass of roadway and enhanced the utilization efficiency of explosive energy. The research findings of this study provide important implications for similar blasting excavation projects.

Keywords: Underground roadway; Overbreak; Underbreak; Blasting excavation; 3D laser scanning; Numerical modeling

1 Introduction

With the increasing demand for natural resources, underground tunnels have been widely constructed in mining engineering for providing crucial access to extract the mineral resource in depth. Although the application of mechanical excavation methods like tunneling boring machines is increasing rapidly, drill-and-blast (D & B) method is still the most popular excavation technique adopted for tunneling due to its low cost and high feasibility of implementation (Cheng et al., 2021, 2022; Lu et al., 2012; Verma et al., 2018; Wang et al., 2021; Zhu et al., 2019). However, this excavation method has an intrinsic shortcoming of causing inevitable damages to the remaining rock mass. The overbreak is one of the critical challenges countering in D & B excavation, which was defined as the surplus breakage of rock beyond the desired tunnel profile (Jang & Topal, 2013). Additionally, the underbreak accompanied by overbreak is defined as the unremoved rock within the designed contour line (Chen et al., 2021). The occurrence of overbreak and underbreak

* Corresponding author.
E-mail address: mingtao@csu.edu.cn (M. Tao).

https://doi.org/10.1016/j.undsp.2022.04.007

in underground projects may result in many issues such as tunnel instability, higher construction and post-blast maintenance costs. Hence, it is crucial to minimize and prevent overbreak and underbreak for the sustainable application of the D & B method in deep tunneling.

Various researches have focused on the factors influencing overbreak and underbreak. The earliest report can be traced back to the study conducted by Hagan (1982), in which the smooth blasting technique was suggested to greatly controlled overbreak. Subsequently, Ibarra et al. (1996) carried out an overall study on overbreak and underbreak. Based on their study, the influencing factors were divided into two categories, so-called geological and blasting factors. On the other hand, Mottahedi et al. (2018) reported that the overbreak causing factors were classified into controllable and uncontrollable, as well as semi-controllable factors. The controllable factors refer to the blasting parameters such as the explosive characteristics, delay time, charge concentration and decoupled coefficient as well as hole stemming which can be adjusted by engineers. The uncontrollable factors denote the geological parameters, or more specifically, the in situ stress field, topography, rock strength, and jointing, etc. (Jang & Topal, 2013). The semi-controllable parameters usually refer to tunnel geometry and size (Mahtab et al., 1997).

For a better understanding of the importance of each factor on the overbreak and underbreak, extensive experimental and theoretical as well as numerical studies have been conducted over the past 50 years (Ganesan & Mishra, 2021; Mahtab et al., 1997; Pal & Shahri, 2014; Rustan, 1998). Hagan (1982) stated that at least four identifiable mechanisms were responsible for blast-induced overbreak, including radial fracturing, internal spalling, gas extension of natural discontinuities and strain wave-induced cracks, and stress transient release fracturing. By performing a numerical and field study, Chakraborty et al. (1994) concluded that the joint orientation considerably influenced the overbreak zone, and the contour blasting technique was of great significance in weak rock masses for minimizing overbreak. Using the small-scale similarity experiments of blasting, the effects of the rock mass features, explosive characteristics and blasting design parameters on overbreak were evaluated, and therefore a new approach for a rational design of the perimeter hole pattern and charge concentration was proposed despite the unchangeable rock mass features (Singh & Xavier, 2005). Regarding the explosive characteristic, a comparison of the overbreak and underbreak between ammonium nitrate fuel oil (ANFO) and emulsion explosive was performed in a deep mine. The results revealed that the magnitude of the overbreak caused by ANFO was larger than that by emulsion. By contrast, the underbreak caused by emulsion was more than that by ANFO (Widodo et al., 2019). Furthermore, Chen et al. (2021) explored the effect of initial support and advance per round on blasting-induced overbreak, and subsequently, an advancing technique using the long and short associate contour blastholes was developed to diminish the overbreak. A long-term study performed by Read (2004) at AECL's Underground Research Laboratory indicated that the in situ stress ahead of the tunnel face influenced the characteristics of overbreak at the excavation perimeter.

By considering the various influencing factors, many researchers have attempted to propose approaches to predict the extent of the overbreak and underbreak (Dey & Murthy, 2012; Mohammadi et al., 2015; Murthy et al., 2003). For instance, taking rock mass rating index (RMR) and borehole length into account, Foderà et al. (2020) presented an empirical model for overbreak prediction by conducting a case survey in three different tunnels. Artificial neural network, one of the important branches of artificial intelligence (AI), has become a wide utilization in overbreak prediction (Koopialipoor et al., 2019). Jang and Topal (2013) proposed three overbreak predicting models using linear and nonlinear multiple regression analysis as well as artificial neural network (ANN). Among them, ANN exhibited the best performance with a coefficient correlation of 0.945. Furthermore, machine learning algorithms including neuro-fuzzy inference system (ANFIS) and Bayes discriminant analysis theory (BDA) are employed to forecast the overbreak value of underground openings (Gong et al., 2008; Mottahedi et al., 2018). As foregoing discussed, the present researches have considerably facilitated the development of the overbreak and underbreak control concerning their causing factor and prediction models. However, only limited reports towards revealing the mechanism and providing guidelines for the blast-induced overbreak and underbreak with respect to a specific underground project have been found (Kim et al., 2003; Kim & Moon, 2013).

In this study, a specific case of the deep Kaiyang Roadway was investigated using the three-dimensional (3D) laser scanning technique, where the combined effect of in situ stress and blasting operation caused the overbreak and underbreak. Then, a simplified 3D numerical model in ANSYS/LS-DYNA code was proposed to simulate the evolution of the rock damages induced by the field blasting experiment. Based on the proposed numerical model, the influences of the in situ stress conditions and blasting parameters including hole spacing, charge concentration and decoupled coefficient as well as stemming were assessed. The findings obtained from this study provide a guideline for minimizing the extent of the overbreak and underbreak.

2 Engineering background

2.1 Site description

The field investigation of the overbreak and underbreak control was conducted in a development roadway in the Kaiyang phosphate mine, which is located in Guiyang city, China. This mine commenced production in 1958, and now has an annual production capacity of six million tons of

raw phosphate ore. With the demand for resources increasing, this mine is currently operating at a buried depth around 800 m, and the backfilling mining method that is accompanied by ore recovery and uses backfilling materials to fill the goaf to ensure the stability of the stope has become the primary method of recovering resources (Fig. 1(a)).

Unfortunately, several mining-induced instabilities have been discerned in mining stopes and some large caverns, leading to greater support costs and lower advancement rates as well as safety problems. The dolomite and sandstone occasionally appear in the test region. S-620, a development roadway with a three-center arch section in Level 620, was selected as the test object. Within 10 m of the test area, five joints whose average length, width and spacing are 1.8 m, 5 mm and 1.5 m were observed in rock mass around the roadway according to the field detection method. Furthermore, the test roadway has been schemed through the Sinian period sedimentary rock area. The geometry of the S-620 is shown in Fig. 1(b) and its width and height are 4200 mm and 3500 mm, respectively.

The field measurement of in situ stresses was performed by overcoring method. The test results indicated that the horizontal (σ_x) and vertical (σ_y) principal stresses were around 20 and 10 MPa, respectively. The main surrounding rock is dolomite and its physical and mechanical properties were determined experimentally. The physical and mechanical properties of the surrounding rock are presented in Table 1.

Table 1
Physical and mechanical properties of the rock mass.

Material properties	Value
Density ρ (kg/m^3)	2722
P-wave velocity v_p (m/s)	5350
Young's modulus E (GPa)	25.39
Poisson's ratio υ	0.23
Tensile strength σ_t (MPa)	7.65
Uniaxial compression strength σ_c (MPa)	108.2
RQD (%)	73
RMR	62

2.2 Blasting design parameters

Considering the geological parameters and roadway geometry, the full-face excavation method was adopted using the D & B method. From the inner to the outer, there were cut holes (red circle), stope holes (green circle), buffer holes (blue circle), and contour holes (black circle) in sequence, as shown in Fig. 2. The millisecond delay technique with nonel detonators was employed to accurately control the initiation time of each blasting row. In the present drilling pattern, the wedge cutting method was used to form the cut zone with the following advantages: lower inhibitory effect of in situ stress on rock fracturing, and larger excavated volume. The original blasting design parameters are listed in Table 2. During the blasting practice, the mining engineers drilled the contour blastholes with a spacing of around 1000 mm to shorten the drilling duration, which exceeded the reasonable value, and the burden width was set as 400 mm.

Due to the application of a rock drilling rig, the charge structure of all boreholes was coupled and successive. As shown in Fig. 2(c), a roll of finished emulsion explosive was charged at the borehole bottom, and then the mixed emulsion explosive was pumped into boreholes through a retractable pipe. The density of mixed explosive ranged from 1.1 to 1.3 g/cm^3, the explosive strength was more than 275 mL, while its detonation velocity was higher than 4000 m/s. Finally, the delayed electronic detonators were used to initiate the explosive. The overall situation of the test roadway including drilling, charging, initiation and measurements of blasting excavation is presented in Fig. 3.

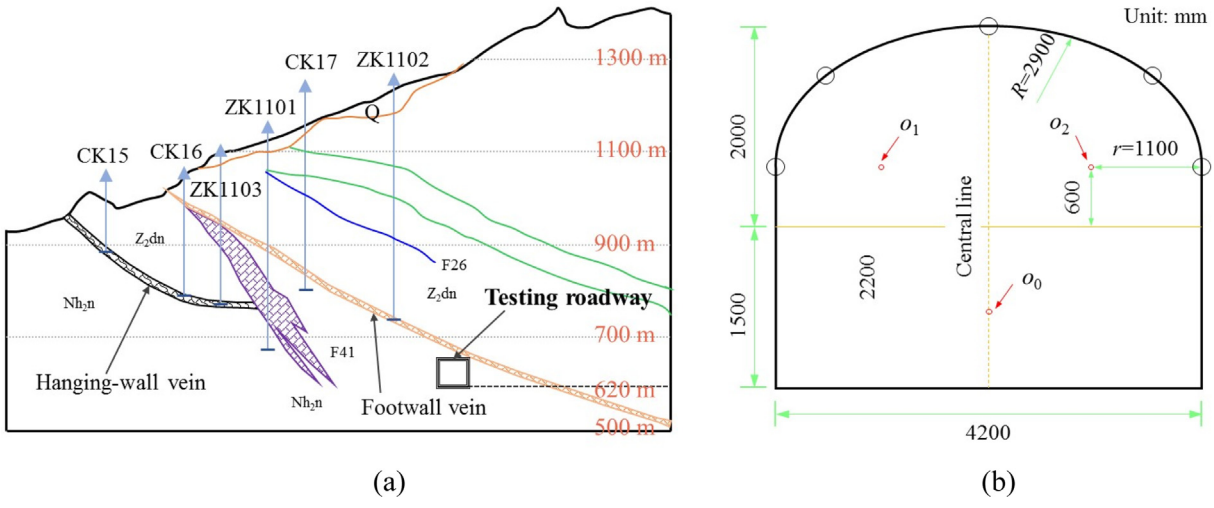

Fig. 1. Configuration of the testing roadway. (a) Drawing exploration section, and (b) geometry of test roadway.

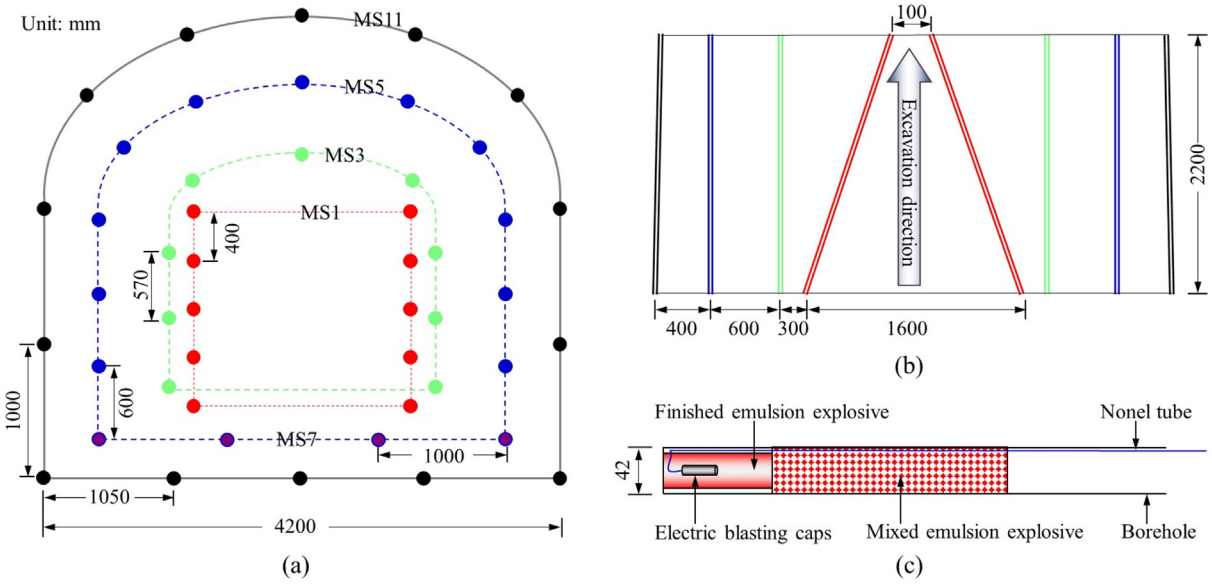

Fig. 2. Schematic diagram of boreholes layout. (a) Front view, (b) top view, and (c) charging structure.

3 In situ measurements and result

3.1 Monitoring equipment

Several methods including manual measurement, standard surveying, photographic sectioning, and light sectioning have been employed in the past to measure the overbreak and underbreak in underground tunnels (Warneke et al., 2007). Nevertheless, some limitations such as subjectivity, high labor-intensity, time-consuming and low accuracy exist in these foregoing methods. In this study, Focus^S 150 laser scanner, a portable non-contact measurement system to accurately capture 3D point cloud data, was employed to scan the roadway profile. This scanner is being widely used in architecture, construction and engineering because it could rotate 360° and measure the roadway geometry within its line of slight with a scan rate of up to 976 000 points per second. The scanning radius ranges from 0.6 m to 150 m, and the measurement duration per round is around 5 min with an accuracy up to ±1 mm (10% reflectance) and 0.6 mm (90% reflectance) at an angle of incidence of zero at 25 m. Table 3 shows the detailed specifications of the Focus^S 150 scanner.

This type of scanner uses the phase-based time of flight measurement. It emits modulated laser light, which means that the frequencies of the light are controlled and known. A phase is a specific location within the wave cycle of the modulated laser light. When the light returns to the scanner, the difference between the phases of the emitted laser light and their turning laser light is calculated, as depicted in Fig. 4. Thus, the distance from the scanner to the object can be accurately determined by the phase shifts in the waves of the infrared light, shown as below:

$$t = \theta/(2\pi f), \tag{1}$$

$$d = ct/2, \tag{2}$$

where t is the time from emission to reception of laser light, θ is the phase shift, f is the frequency and c is the speed of light.

3.2 Test procedures

The schematic diagram of the 3D laser scanning is presented in Fig. 5. The test procedures of field measurements can be divided into the following steps. First, a coordinate reference point in the roadway roof in front of the excavation face is set, and then the total station is used to measure the absolute coordinates. The function of the coordinate reference point is to provide the target balls with coordinates. Subsequently, four target balls were mounted at the two sidewalls in front of the excavation face to allow the scanner processing software to merge adjacent scans. Finally, the 3D laser scanner is placed on a tripod, and adjusted in the horizontal plane. Meanwhile, turn on the scanner beginning to scan the roadway profile, and save

Table 2
Designed parameters of original blasting pattern.

Blasthole	Spacing (mm)	Burden (mm)	Charge (kg)	Length (mm)	Angle (°)
Cut hole	400	–	2.8	2324	19
Stoping hole	570–600	300/600	2.3	2200	0
Smooth hole	1000–1050	400	1.8	2220	2

Fig. 3. Blasting operation and field measurement of the test roadway.

Table 3
Performance specifications of Focus^S 150 scanner.

Ranging unit	
614 m for up to 0.5 mil. pts/s 307 m at 1 mil. pts/s	
Range	
90% Reflectivity (white) (m)	0.6–150
10% Reflectivity (dark-gray) (m)	0.6–150
2% Reflectivity (black) (m)	0.6–50
Range Noise	
Max. measurement speed (mil. pts/s)	up to 1
Ranging error (mm)	±1
Angular accuracy	19 arcsec for vertical/horizontal angles
3D Point accuracy	2 @10 m 3.5 @25 m
Laser (Optical Transmitter)	
Laser class	Laser Class 1
Wavelength (nm)	1550
Beam divergence (mrad)	0.3 (1/e)
Beam diameter at exit (mm)	2.12 (1/e)
Deflection Unit	
Field of view horizontal	300° vertical/360° horizontal
Max. scan speed (Hz)	97 (vertical)

the 3D point cloud data. When the second blasting round is completed, move the laser scanner and target balls along the advancement direction for 2.2 m, and repeat the above steps.

3.3 Results and analyses

In this study, based on the original blasting scheme described in Table 2 and Fig. 2, a representative measurement result was selected to analyze the overbreak and underbreak around the underground roadway. As shown in Fig. 6(a), four half-barrels were observed at roadway crown and sidewall upon contour blasting. Saiang (2008) reported that the technique factors were the main components contributing to the overbreak and underbreak as they occurred in a zone of visible half-barrels. Thus, it is feasible to diminish the influence of blast-induced damage by optimizing the current blasting design. The point cloud map of the post-blast roadway is presented in Fig. 6(b), in which four target balls (TB1-4) were observed on the sidewalls. The point cloud map revealed that regions with hollows and protrusions were unevenly distributed on the roadway surface, indicating the occurrence of overbreak and underbreak. To obtain the distribution and magnitude of the overbreak and underbreak around the roadway, the preprocessing software SCENE was used to deal with the point cloud data. Afterward, Trimble Business Center was employed to generate laser scanning images and provide accurate quantitative analysis reports. Along the opposite direction of advance, five sections (Fig. 6(c)) were extracted for presenting the extent of overbreak and underbreak surrounding the test roadway.

The measurement results of five roadway sections are presented in Fig. 7. Figure 7(e) reports that the maximum

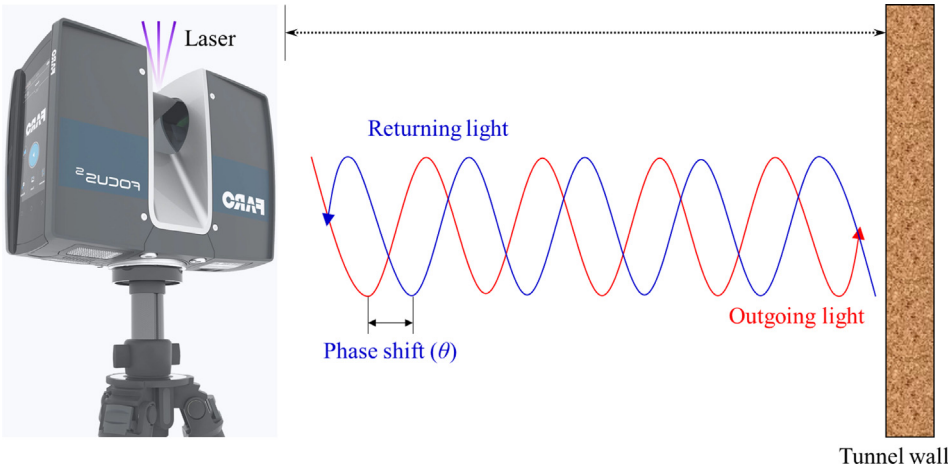

Fig. 4. Principle of distance measurement.

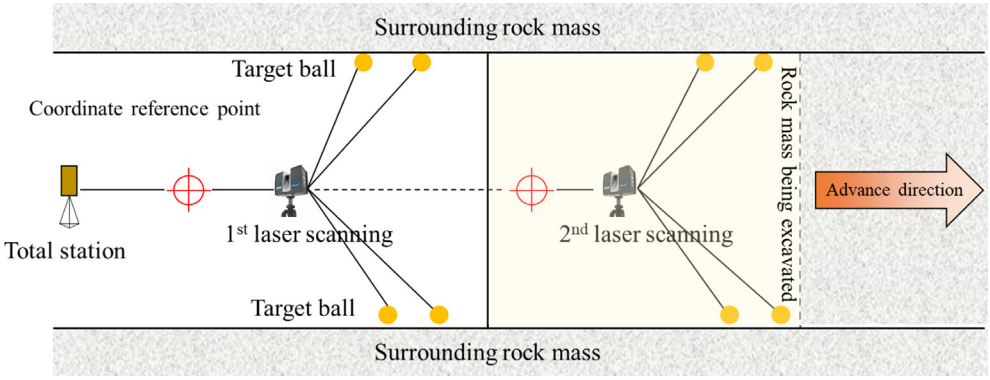

Fig. 5. Schematic diagram of the 3D scanner scanning station (Li et al., 2021).

extents of the overbreak and underbreak were 11.3 and 31.6 cm, respectively. The overbreak extents at the roadway roof and sidewalls were below the tolerance, which indicated that the surrounding rock mass in Section-5 was slightly damaged owing to the high energy utilization rate. However, a large region of underbreak was observed near the roadway floor, and it can be explained by the fact that rock mass on the floor was subjected to larger resistance at the borehole bottom than that at sidewalls and roofs.

Figure 7(d) indicates that the maximum extents of overbreak and underbreak were 39.1 cm and 13.1 cm. The overbreak extent was larger at the roadway roof than that at the roadway sidewall. Furthermore, as Section-4 was the center of the charge volume, a larger extent of overbreak was induced at the roadway crown due to the superposition of blasting stress waves, which greatly exceeded the tolerance value and aroused a potential threat to the roadway stability.

Figure 7(c) illustrates that the magnitude and distribution of overbreak and underbreak were essentially identical to those in Section-5. Since blastholes were not stemmed, most of the explosion energy was carried away by the explosion gases so that the blasting pressure was rapidly attenuated. Consequently, in Section-2 shown in Fig. 7(b), the maximum value of overbreak was 35.8% lower than that at $y = 1.0$ m. When it was near the borehole orifice (Section-1), although the pressure on the borehole wall decreased below the dynamic compressive strength of rock, a relatively ideal blasting result was achieved under the action of reflected tensile waves. The maximum underbreak and overbreak were 31.4 cm and 7.4 cm, respectively.

To quantitatively analyze the normal distribution of the overbreak and underbreak, the dispersion information of the overbreak and underbreak at different sections are presented in Fig. 8. First, the variation in the mean overbreak indicated that the overbreak extent increased and subsequently decreased with the excavation advance. On the contrary, the underbreak extent showed a trend that decreased and subsequently increased with the excavation advance. Thereafter, the values of overbreak at Section-5 were concentrated in the range 2.32–9.65 cm, while the values at Section-4 were extremely discrete with a difference of around 36 cm. The values of underbreak at Section-1 mainly ranged from 4.36 to 16.75 cm. Moreover, a majority of the roadway excavation contour was in the state of overbreak, with a maximum extent of approximately 40 cm. It is concluded that the minimum overbreak occurs at the blasthole bottom, while the overbreak extents are concentrated in the range of charge section.

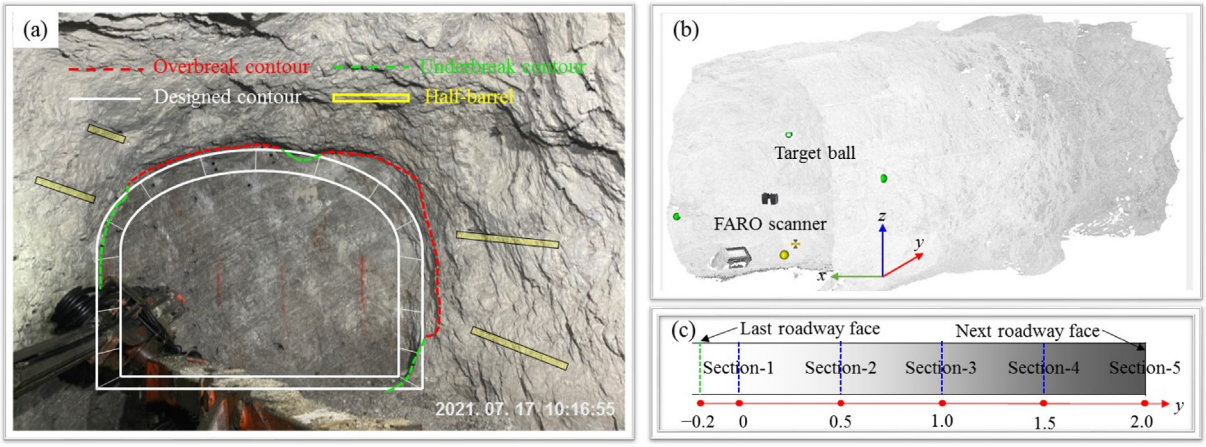

Fig. 6. Overall blasting result. (a) photo of the post-blast roadway, and (b) point cloud map, and (c) schematic diagram of the selection of roadway section (Unit: m).

In conclusion, the measurement results indicated that the evident overbreak and underbreak appeared in the excavation contour when using the original blasting pattern. Moreover, the place where the maximum underbreak appeared was the roadway floor due to these rocks being in the high in situ stress concentration and difficulty in breaking. The mining engineer of Kaiyang mine reported that the cost of the support system has increased by around twenty percent, and the construction schedule has been seriously delayed owing to the overbreak and underbreak damage. Therefore, it is urgent to improve the blasting result by optimizing the blasting parameters whereas the geological parameters remain unchanged.

4 Numerical model and calibration

The overbreak and underbreak of the test roadway excavated by the original blasting scheme were analyzed by field measurement, and it was indicated that optimizing the original blasting scheme is necessary to minimize the influence of blasting excavation damage. As the full-scale field experiments are time-consuming and expensive, numerical simulation technique was therefore used to provide further insight into the mechanism and investigate the effects of influencing factors on the extent of overbreak and underbreak. In the present study, the overbreak and underbreak in the surrounding rock of the test roadway under various optimized blasting parameters were simulated using the dynamic finite element program LS-DYNA.

4.1 Numerical model

As reported by Holmberg (1979) that the last row of blastholes from the perimeter was producers of overbreak as the blastholes were charged heavily. Therefore, a simplified 3D numerical model was established based on an assumption that the influences of cutting and stopping blasts on the overbreak and underbreak are ignored. It had a geometrical size of 20 m × 20 m × 5 m with around 5.6 million hexahedral elements, as shown in Fig. 9. The smallest element with the size of 0.022 m × 0.0093 m × 0.067 m was meshed in the region near the contour boreholes. The blasting parameters used in the numerical model were identical to those in the blasting practice, in which the borehole had a diameter of 42 mm, with a spacing of 1.05 m, and a burden of 0.4 m. Free boundary and non-reflecting boundary were set on the outer faces of the model in combination with the actual scenario. The in situ stresses imposed on the model in the horizontal and vertical directions perpendicular to the roadway direction were 20 and 10 MPa by employing the Restart technique. Moreover, a massively parallel processing (MPP) version of the LS-DYNA solver was used to calculate this model because of the great number of elements.

4.2 Material models

4.2.1 Rock mass

Developing constitution models for describing the dynamic mechanical behavior of rock under impact load has always been a hot and difficult issue for scholars. Fortunately, remarkable achievements have been made in the research of the constitution model for brittle materials with complex mechanical behavior after great effort. Many material models in the material library of LS-DYNA, such as MAT_PLASTIC-KINEMATIC, MAT_CONCRETE_-DAMAGE_REL3, MAT_CSCM and MAT_RHT, have been used to simulate the dynamic responses of rock mass and concrete. Considering the effects of both compression and tension on the surrounding rock mass that is subjected to coupled static and dynamic loads, the MAT_RHT constitution model was selected in this study to mimic the blast-related rock damage surrounding the underground roadway.

RHT is an advanced damage plasticity model for brittle materials, which was first proposed by Riedel et al. (1999) for studying the dynamic loading of concrete and then

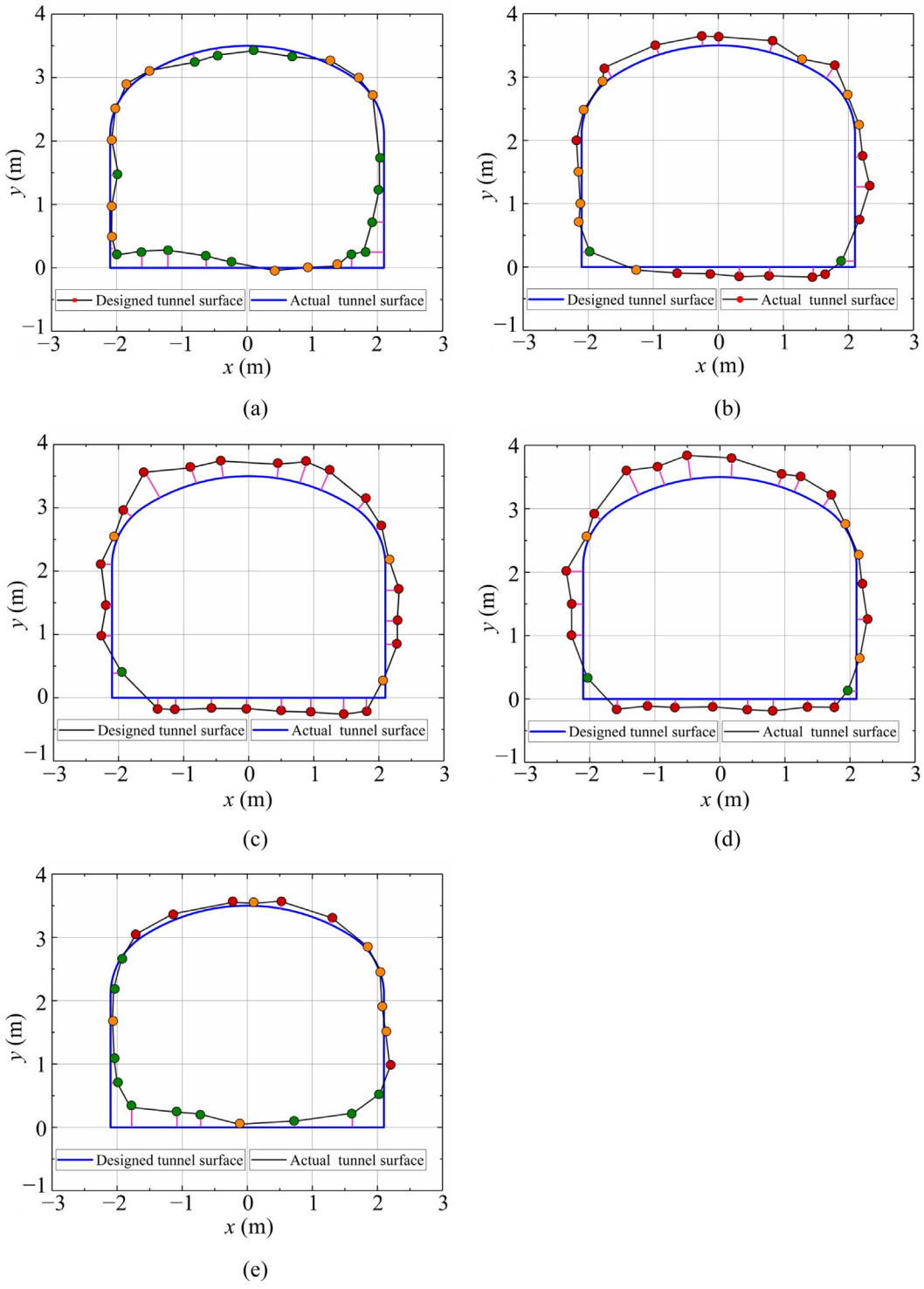

Fig. 7. Measurement results of overbreak and underbreak in five sections of the test roadway. (a), (b), (c), (d) and (e) are Section-1 to Section-5 in sequence. Red and green points respectively represent overbreak and underbreak with a value greater than 0.1 m, and orange point represents overbreak or underbreak less than 0.1 m (Unit: m).

implemented in LS-DYNA code in 2011 (Borrvall, 2011) for modeling more brittle materials. As depicted in Fig. 10, three limit surfaces including failure surface, yield surface and residual surface are involved in the RHT model which describes the material strength model. It is important to emphasize that when the stress reaches the residual surface, the material is considered to be fully damaged, and the strength is determined by a residual surface. More detailed information about the RHT model was given by Yi et al. (2018, 2021, 2017).

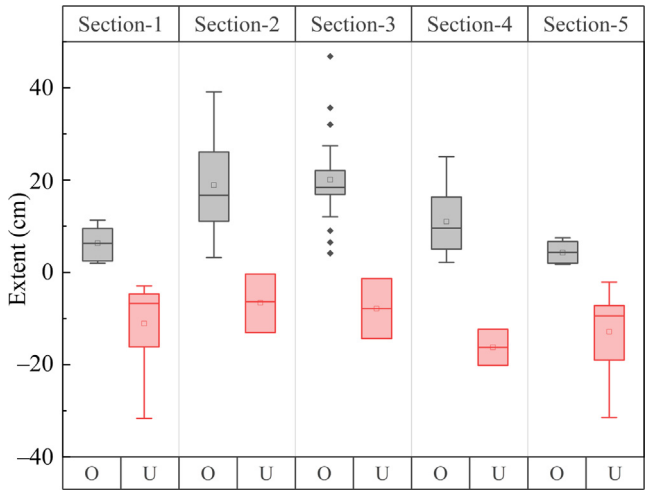

Fig. 8. Box-plot of overbreak and underbreak extents in five sections. ("O" represents overbreak, and "U" represents underbreak).

In the RHT model, the damage degree is defined as follows:

$$D_{\mathrm{f}} = \sum \frac{\Delta\varepsilon^{\mathrm{p}}}{\varepsilon^{\mathrm{f}}}, \tag{3}$$

where $\Delta\varepsilon^{\mathrm{p}}$ is the accumulated plastic strain, and ε^{f} is the failue strain written as

$$\varepsilon^{\mathrm{f}} = D_1\left(\frac{p}{f'_{\mathrm{c}}} - \frac{p_{\mathrm{spall}}}{f'_{\mathrm{c}}}\right)^{D_2}, \tag{4}$$

in which D_1 and D_2 are initial damage parameters given by the user; p and p_{spall} are pressure and spalling strength, respectively; f ' c is the uniaxial compression strength.

Significantly, the damage factor $D_{\mathrm{f}} = 1$ indicates absolute damage to rock mass, while $D_{\mathrm{f}} = 0$ means undamaged. The basic RHT parameters used in this study were obtained by rock mechanics experiments on-site and laboratory. Furthermore, other sensitive variables were determined in terms of true triaxial test and high strain rate impact test conducted in Central South University. Constant trial calculations are essential in the process of determining rational rock parameters. The input parameters are listed in Table 4.

4.2.2 Explosive and air

The emulsion explosive used in field blasting operation was modeled by MAT_HIGH_EXPLOSIVE_BURN in LS-DYNA (Material Type 008) together with the Jones-Wilkens-Lee (JWL) Equation-of-State (EOS). This EOS is widely used to calculate the detonation pressure for detonation products. JWL EOS is expressed as (Liu et al., 2019)

$$P = A\left(1 - \frac{\omega}{R_1 V}\right)\mathrm{e}^{-R_1 V} + B\left(1 - \frac{\omega}{R_2 V}\right)\mathrm{e}^{-R_2 V} + \frac{\omega E}{V}, \tag{5}$$

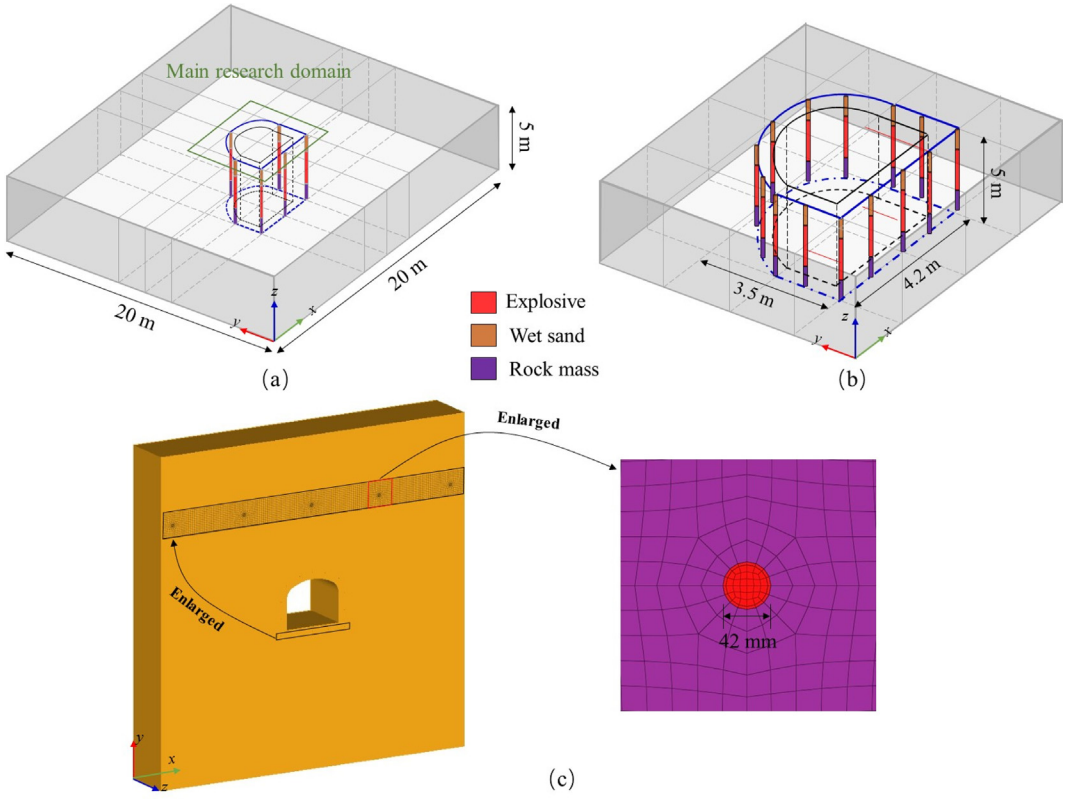

Fig. 9. Configuration of the numerical model and finite element mesh. (a) integral model, and (b)main research domain, and (c) finite element mesh of the integral model and rock adjacent to borehole.

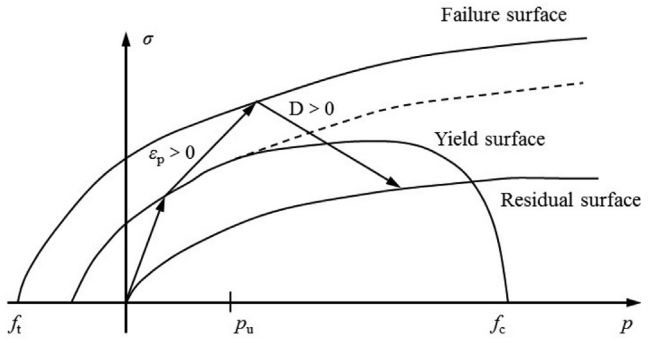

Fig. 10. Schematic diagram of three surface concepts in the RHT model.

where P is the pressure of detonation products; A, B, R_1, R_2 and ω are the material constants; V is the relative volume; E is the specific energy with an initial value of E_0. In the present study, the basic physical and mechanical parameters of the explosive were provided by the product manufacturer, and the JWL EOS was referred to the literature (Liu et al., 2019). The parameters of emulsion explosives are listed in Table 5.

The air modeled by combining MAT_NULL (Material Type 009) and a linear polynomial EOS in LS-DYNA was used for subsequently simulating the effect of decoupled charging on the control of rock damage. The EOS is written as (Liu et al., 2018)

$$P = \left[C_0 + C_1\mu + C_2\mu^2 + C_3\mu^3\right] + \left[C_4 + C_5\mu + C_6\mu^2\right]E_0, \quad (6)$$

where C_0, C_1, C_2, C_3, C_4, C_5, and C_6 are polynomial equation coefficients, and E_0 is the initial internal energy per unit reference volume. The compression of material is defined by the parameter $\mu = (\rho/\rho_0) - 1$ with ρ and ρ_0 being the current and initial density of air, respectively. In the present study, the air was modeled with the gamma law equation of state. This can be achieved by setting $C_0 = C_1 = C_2 = C_3 = C_6 = 0$, and $C_4 = C_5 = \gamma - 1$, in which γ is the ratio of C_p to C_v.

4.2.3 Stemming material

In this study, to investigate the influence of stemming conditions on overbreak and underbreak around the underground roadway, the material type 5 of LS-DYNA (MAT_SOIL_AND_FORM) was used to simulate the dynamic response of wet sand which is used in Section 5.5. This model does not consider the strain harden characteristic, and its yield limit is only related to pressure p. On the yield surface, the uniaxial yield stress is expressed as

$$\sigma_y = \left[3\left(a_0 + a_1 p + a_2 p^2\right)\right]^{0.5}, \quad (7)$$

where a_0, a_1, and a_2 are constants for plastic yield function, and p is the pressure. The specific material parameters are listed in Table 6.

4.3 Numerical calibration

The above numerical model matching with the materials was used to simulate the field measurement in Section 3. The simulated results of rock damage induced by the contour blasting of the D-shaped roadway are shown in Fig. 11. It can be seen from Fig. 11(a) that the rock mass in the designed excavation area is damaged in general, and rock damages between each borehole have completely coalesced. However, we can see obviously that near the explosive charge zone, the rock is over-damaged, thus indicating the appearance of overbreak. Furthermore, it can be seen from Fig. 11(b) that the integrity of rock mass near Section-1 is good, in other words, it suffers a slight impact from the contour blasting excavation. This is probably because the mechanical properties of rock near the roadway surface are not degraded accordingly, which is inconsistent with the practical situation. To intuitively compare the simulation results with the field measurement results, five sections were extracted from the model.

Since the model is symmetrical about the y-axis, the right half of the rock damage contour was selected for analysis, as shown in Fig. 12. It is obvious that the damage

Table 4
RHT constitution parameters for dolomite.

Parameter	Value	Parameter	Value
Mass density ρ_0 (kg/m^3)	2722	Tensile strain rate dependence exponent β_t	0.042
Shear Modulus G (GPa)	10.32	Pressure influence on plastic flow in tension ζ	0.001
Compressive strength f_c (MPa)	108.2	Compressive yield surface parameter G_C^*	0.85
Eroding plastic strain EPSF	2.00	Tensile yield surface parameter G_T^*	0.40
Parameter for polynomial EOS B_0	1.22	Shear modulus reduction factor ξ	0.50
Parameter for polynomial EOS B_1	1.22	Damage parameter D_1	0.04
Parameter for polynomial EOS T_1 (GPa)	35.27	Damage parameter D_2	1.00
Failure surface parameter A	1.80	Minimum damaged residual strain ε_p^m	0.01
Failure surface parameter N	0.71	Residual surface parameter A_f	1.60
Relative shear strength f_s*	0.07	Residual surface parameter N_f	0.61
Lode angle dependence factor Q_0	0.68	Hugoniot polynomial coefficient A_1	35.27
Lode angle dependence factor B	0.01	Hugoniot polynomial coefficient A_2 (GPa)	39.58
Compressive strain rate β_c	0.032	Hugoniot polynomial coefficient A_3 (GPa)	9.04
Reference compressive strain rate εc 0	3.0×10^{-5}	Crush pressure P_{el} (GPa)	0.0233
Reference tensile strain rate εt 0	3.0×10^{-6}	Compaction pressure P_{c0} (GPa)	6.0
Break compressive strain rate ε_c	3.0×10^{25}	Porosity exponent N_p	3.00
Break tensile strain rate ε_t	3.0×10^{25}	Initial porosity α_0	1.00

Table 5
Emulsion explosive parameters.

ρ_e (kg/m^3)	VOD (m/s)	P_{cj} (GPa)	A (GPa)	B (GPa)	R_1	R_2	ω	E (GPa)
1120	4200	9.7	42	0.44	3.55	0.16	0.41	0.71

zone of the surrounding rock mass first increases then reduces with the increase of excavation advance, which agrees well with the field measurement results. At the center of charge area, besides the region desired to be excavated, a greater region beyond the designed roadway profile is damaged severely, which is termed as overbreak in rock engineering. As shown in Fig. 12(a), the overbreak extents at roadway crown, floor and sidewall are 22.03, 18.62 and 24.13 cm, respectively. That is to say, the rock masses around boreholes were damaged severely, while the rock damages or cracks did not coalesce with each other. Therefore, the rock within the burden was not stripped away from the host rock owing to the lack of enough blasting load, that indicates an obvious underbreak zone. The phenomenon of greater underbreak zone and smaller overbreak zone in the simulation can be attributed to the neglect of the significant reduction of the mechanical properties of rock around roadway face, which is inconsistent with the practical situation.

Figure 12(c) shows the rock damage contour of Section-3. The overbreak extents at roadway crown, floor and sidewall are 27.21, 27.22, and 28.94 cm, respectively. In addition, an underbreak zone with an extent of 8.65 cm was generated in the corner of the roadway bottom. Compared with the corresponding measurement results, both the deviations are less than 20%. Therefore, it is concluded that the above model and materials are effective in mimicking the blast-induced rock damage around a deep roadway.

Figure 12(d) shows the rock damage contour of Section-4. Because Section-4 locates at the center of the blasthole charge, an overbreak zone with a depth of 53.87 cm was induced at the roadway sidewall owing to excessive explosion wave stress, which is 37.7% greater than the measurement result. The rock mass in the burden was fully distrusted, implying that no underbreak zone emerged around the roadway. It is noteworthy that the place of maximum overbreak transforms from the periphery of the contour holes to the middle section of two adjacent boreholes, which can be attributed to the superposition of blast-induced stress waves.

As seen in Fig. 12(e), the rock mass within the burden was completely fractured except for that in the vicinity of the roadway corners, and extra damage was observed in the surrounding rock mass, indicating that overbreak was induced during the blasting excavation. The overbreak extents at roadway crown, floor and sidewall are 18.49, 30.85, and 28.77 cm, respectively. However, similar to the damage contour in Fig. 12(c), a small underbreak zone was observed at the corners of the roadway bottom. A comparison between the simulated and field measurement results reveal that the distributions of the overbreak and underbreak are generally consistent. The maximum extents of the overbreak and underbreak were 30.85 and 32.7 cm, respectively, which were −19.55 and 1.1 cm differences from the field measurement data in Fig. 7(b).

Via the verification of the scanned data of roadway profile, the simulation result can be considered as a reasonable and accurate prediction of the measurement results. The analysis of the distribution pattern and extents of overbreak and underbreak indicates that the proposed numerical model in this study is applicable and suitable for mimicking rock damage caused by blasting excavation of deep roadway at the site under consideration.

5 Discussion

Although the geological parameters and blasting parameters have been demonstrated to be the two main factors contributing to the formations of overbreak and underbreak in underground tunnels, many attempts have been made to predict the extent of rock damage through peak particle velocity (PPV) and deep learning algorithms. However, experimental or numerical investigations on overbreak control were still rare with respect to the effect of in situ stress. The simplified numerical model in the present study has been proved to be reliable in predicting the extent of rock damage and providing a promising approach to understanding the evolution of blast damage. Thus, a series of numerical simulations were conducted on the basis of the field measurements in the Kaiyang phosphate mine. The geological and blasting parameters including in situ stress conditions, contour hole spacing, stemming, charge concentration and decoupled coefficient are discussed in this section.

Table 6
Main material parameters for wet sand.

Parameter	Value	Parameter	Value
Mass density ρ_0 (kg/m^3)	1800	Yield function constant a_1	3.4×10^7
Shear modulus G (MPa)	63.80	Yield function constant a_2	6.398×10^3
Bulk modulus K (GPa)	1.26	Yield function constant a_3	0.30
Volumetric strain values ε_1	0.00	Pressure cutoff for tensile fracture P_c	-6.9×10^3

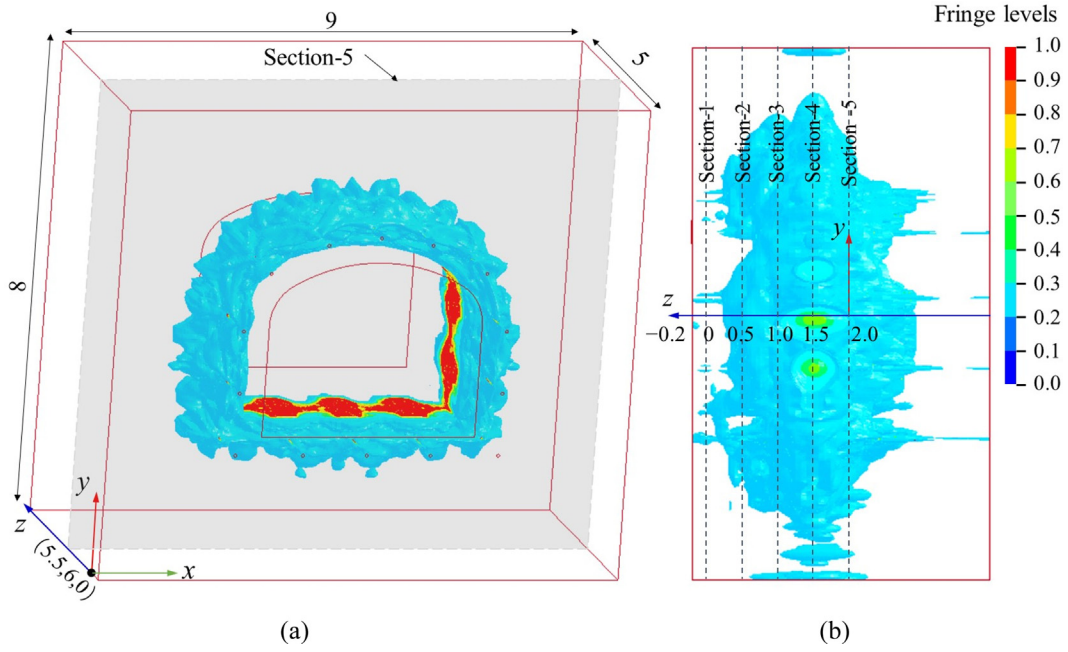

Fig. 11. Damage profile of rock mass around the blast-excavation roadway. (a) Oblique view of rock damage contour, and (b) side view of rock damage (Unit: m).

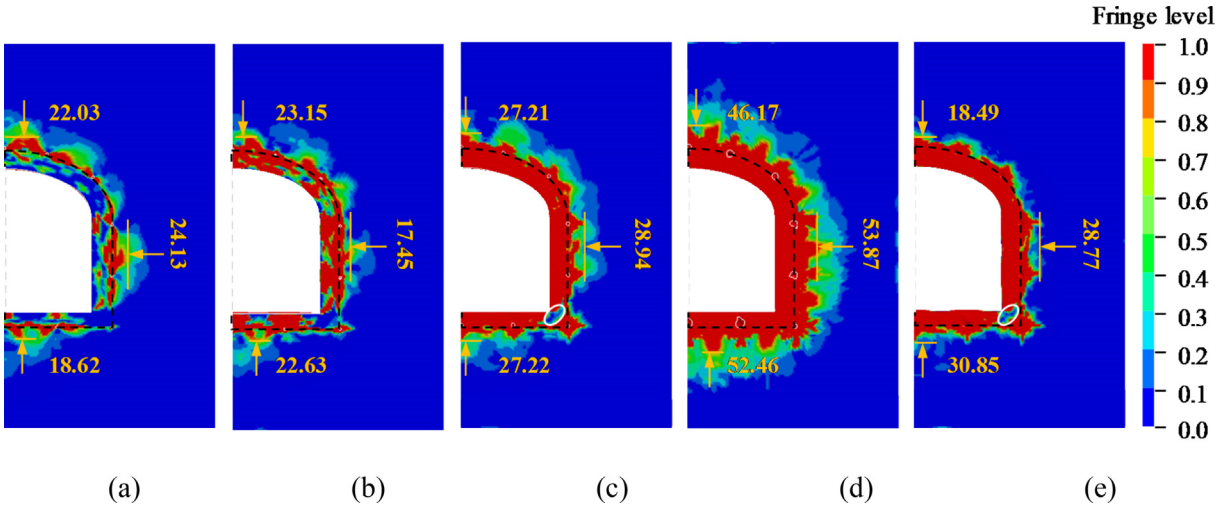

Fig. 12. Numerical results of blast-induced damage at five sections. (a), (b), (c), (d) and (e) are sections 1 to 5 in sequence (Unit: cm).

5.1 Effect of in situ stresses

According to previous studies, in situ stress is an important factor contributing to the extent and distribution of rock damage when rock mass is subjected to the action of blasting (Han et al., 2020; Xie et al., 2019). Thus, it's important to consider the effect of in situ stress when evaluating the overbreak and underbreak around underground openings, particularly under high and complex stress conditions. Keeping the blasting parameters of testing roadway unchanged, two cases with different stress magnitudes and lateral-pressure coefficients were run as follows:

Case 1: $\sigma_x = \sigma_y = 20$, 30, 40, and 50 MPa. This case was set to investigate the magnitude of in situ stress on the extents of overbreak and underbreak;
Case 2: $\sigma_y = 10$ MPa, $\sigma_x = 10$, 30, 40, and 50 MPa. This case was set to investigate the effect of lateral pressure coefficients on the extents of overbreak and underbreak.

In this study, Section-3 and Section-5 were chosen for analyzing the effect of in situ stress on the extents and distributions of the overbreak and underbreak. The final damage zones under hydrostatic and non-hydrostatic pressures conditions are shown in Figs. 13 and 14, respectively. The final excavation damages around roadway under different

hydrostatic pressures are presented in Fig. 13. The magnitude of overbreak is observed to increase with the in situ stress when the in situ stress is less than 30 MPa. Conversely, the magnitude of overbreak slightly decreases with the in situ stress when it is greater than 30 MPa. Under $\sigma_x = \sigma_y = 50$ MPa, the overbreak extent at sidewall in two sections are 22.06% and 16.33% lower than those under $\sigma_x = \sigma_y = 10$ MPa, respectively. It is generally acknowledged that excavation with the D & B method causes a sudden release of in situ stress, which leads to a strong transient dynamic disturbance to the surrounding rock mass, and the rock damage is promoted by the increasing unloading rate. However, because the in situ stress has resistance against the propagating blasting load, the extent of rock damage is yielded in the rock mass under high in situ stress conditions. Thus, the aforementioned phenomenon could be attributed to the superposition of the damage induced by the stress release and blasting load.

When increasing σ_x to 40 MPa, the extent of overbreak at roadway sidewall gradually increases, and the extents of overbreak in Section-5 and Section-3 increase by about 24.25% and 22.43%, respectively, indicating that the lateral pressure coefficient significantly affects the evolution of rock damage in horizontal direction (Fig. 14(a) and (b)). By comparison, the overbreak extents at roadway roof and floor in Section-5 and Section-3 decreased by 30.76%, 30.18%, 22.6%, and 20.77%, respectively. Thus, more attention should be paid to the blasting scheme as the roadway was subjected to a stress field with a higher lateral pressure coefficient. Additionally, it can be seen from Fig. 14(a) and (b) that as for the underbreak that occurred at the corners of the roadway, its extent doesn't vary with the increase of β.

5.2 Effect of hole spacing

It has been demonstrated that too small spacing of contour borehole will create overbreak, while too large will create underbreak. The current technique of blasting damage control is based on closely spaced perimeter holes, and the perimeter hole spacing is determined by semi empirical method (Iverson et al., 2013). It is still a confusing problem what is the most ideal hole spacing for the specific explosive, blasthole diameter and burden. The proper hole spacing for contour blasting is suggested by Hustrulid and Johnson (2008) using rock strength and explosion pressure, which could be expressed as follows:

$$S = 2r_h\left(\frac{P_\omega + \sigma_t}{\sigma_t}\right), \tag{8}$$

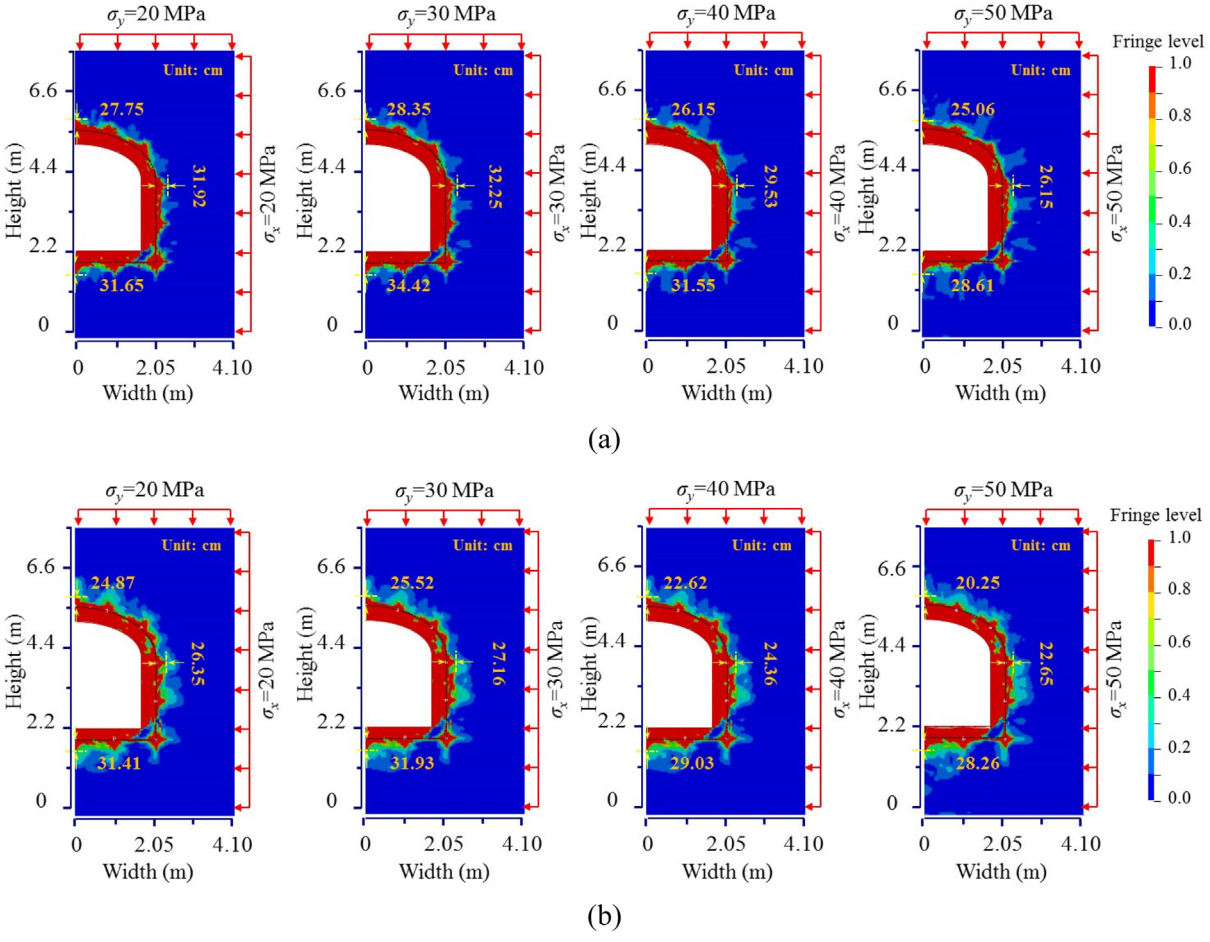

Fig. 13. Numerical results of blast-induced damage of rock within various magnitudes of in situ stress. (a) Section-3, and (b) Section-5.

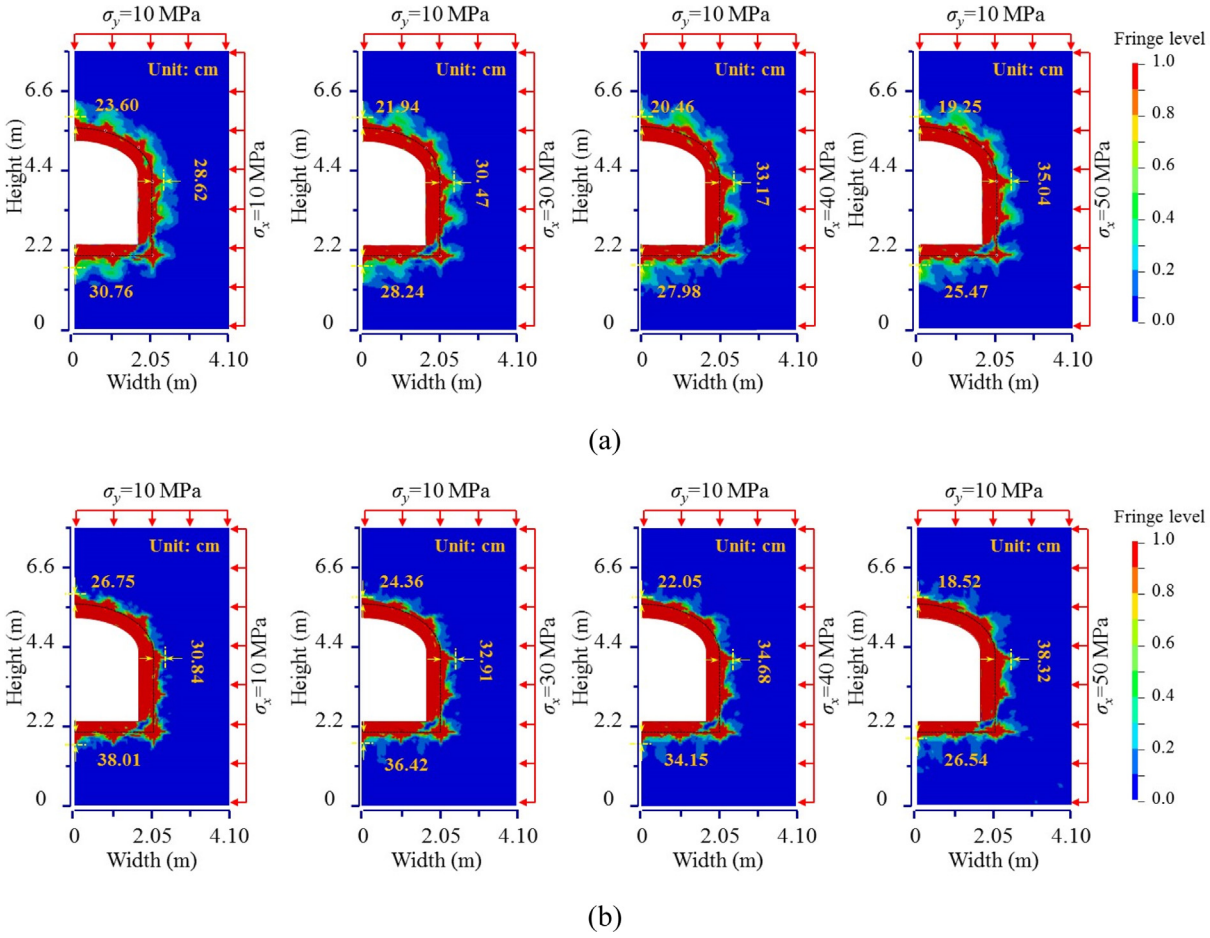

Fig. 14. Numerical results of blast-induced damage of rock within various β. (a) Section-3, and (b) Section-5.

where S is the perimeter hole spacing, r_h is the blasthole radius; P_w is the explosion pressure exerted on the blasthole wall, and σ_t is the tensile strength of intact rock.

Based on this, the hole spacing in contour blasting modelling reduced to 0.84, 0.70, and 0.60 m. The numerical results are presented in Fig. 15. A comparison of Figs. 12 and 15 indicats that in the region where explosive was charged, the magnitude of overbreak near the blasthole perimeter increased while the extent of underbreak decreased with the decrease of S. As presented in Fig. 15 (a), the maximum overbreak was 81.32 cm occurring at the roadway floor in Section-4, and it was almost twice as much as that at $S = 0.84$ m. Note that the rock mass in the roadway roof has not been fractured, and thus a greater underbreak was created at $S = 0.60$ m as compared with that at $S = 0.84$ m, although the thickness of overbreak near the charge center was larger at $S = 0.70$ m than that at $S = 0.84$ m. In terms of the volumes of overbreak and underbreak, at $S = 0.70$ m, both the overbreak and underbreak declined and well controlled. Therefore, it can be concluded that the perimeter hole spacing is not as large or as small as possible. The optimal result using the D & B method was obtained at a spacing of 0.70 m in this blasting case.

5.3 Effect of charge concentration

Charge concentration (β) is defined as the weight of explosive per length of borehole. Previous studies suggested that different values of charge concentration should be employed in a blasting operation depending on the location of the boreholes because the effective choice of charge concentration could lead to the optimal blasting pressure required for adequate rock breakage. The excavation result of the testing roadway indicated that the factor of charge concentration was so large that a big undesirable damage zone around charging boreholes was generated. Herein, the charge lengths were adjusted to 1.5 and 2.0 m without changing the charge weight of 1.8 kg, and the corresponding charge concentration coefficients were 1.2 and 0.9 kg/m.

The final damage pattern under diverse charge concentration coefficients are presented in Fig. 16, indicating distinct rock damage as compared with the numerical results in Fig. 12. In addition to the effective damage of the rock mass in the region from Section-5 to Section-3, the rock mass in the region from Section-3 to Section-1 was damaged to a certain extent, which means a small underbreak zone. The maximum overbreak at sidewall in Section-4 at

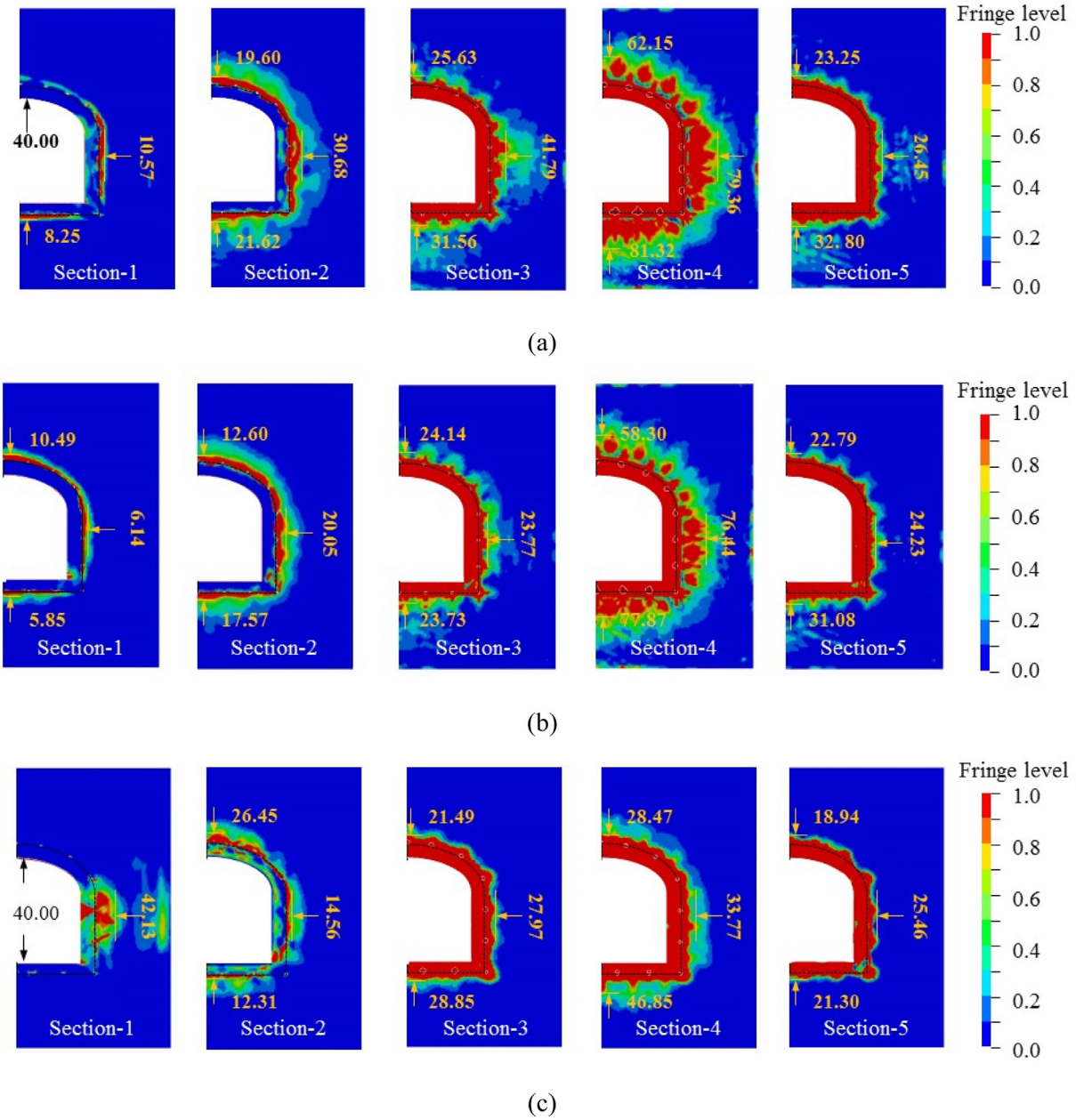

Fig. 15. Numerical results of blast-induced damage of rock within various hole spacing. (a) $S = 0.60$ m, and (b) $S = 0.70$ m, and (c) $S = 0.84$ m (Unit: cm).

$\beta = 0.9$ kg/m was 27.48 cm less than that induced by the original blasting scheme, while it was 8.58 cm lower than that at $\beta = 1.2$ kg/m. Thus, the rock damage caused by blasting was efficiently controlled with the reduction in the charge concentration coefficient. Specifically, the optimal blasting result with respect to the overbreak and underbreak was obtained at β equal to 0.9 kg/m.

5.4 Effect of decoupled coefficient

It is well known that the decoupled charge blasting can improve the action effect of explosion wave and blasting gas, which is significant to avoid the excessive rock damage and control the fragmentation size. In order to analyze the influence of decoupled charge on overbreak and underbreak, the decoupled coefficients were set as 3.0, 2.5, and 2.0 with a constant charge length of 1.0 m, and the final damage pattern around roadway with three decoupled coefficients are presented in Fig. 17. The extent of overbreak is observed to decrease upon increasing the decoupled coefficient. In turn, as the decoupled coefficient ζ increases, the extent of overbreak increases accordingly. Compared with the numerical results in Fig. 12(b)–(f), the charge weight reduces due to the decoupled charge structure, resulting in the increase in underbreak extent in the uncharged section. Specifically, the rock mass in the uncharged section was slightly damaged, which is regarded as a failure of blasting operation. The comparison of the

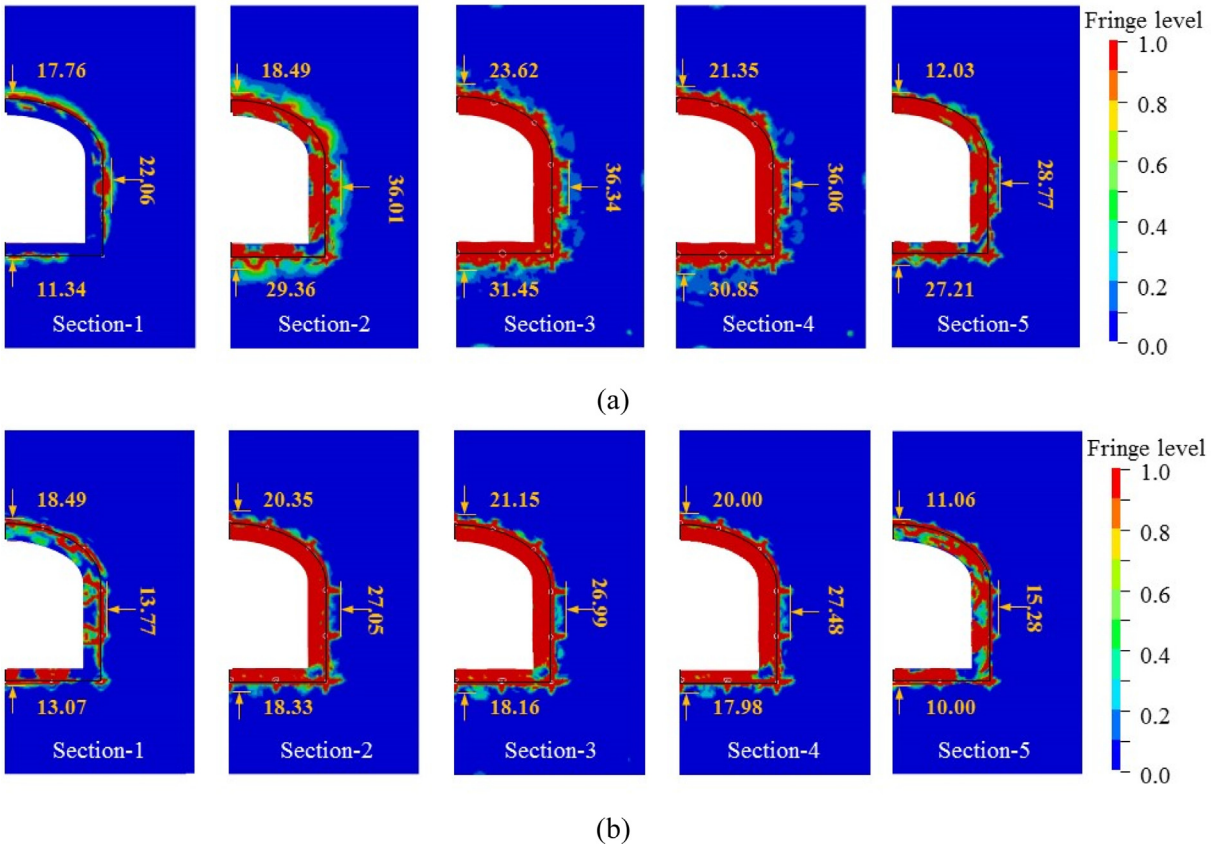

Fig. 16. Numerical results of blast-induced damage of rock at various charge concentrations. (a) $\beta = 1.2$ kg/m, and (b) $\beta = 0.9$ kg/m (Unit: cm).

extents of overbreak and underbreak between Fig. 17(b) and (a) and (c) indicat that at $\zeta = 2.5$, the rock in the burden was almost damaged with the smallest overbreak and underbreak. Therefore, as the charge length is not considered, $\zeta = 2.5$ is the most proper decoupled coefficient for the excavation of the designed profile and control of excessive blasting damage, and it is recommended to be used in contour blastholes of the development roadway in the Kaiyang phosphate mine.

5.5 Effect of blasthole stemming

The previous researches on blasting stemming using experiment and simulation methods illustrated that the stemmed explosive charge increased the energy contained in the stress waves transmitted into rock and produced more and longer radial cracks than that induced by unstemmed charge (Zhang et al., 2020, 2021). Unfortunately, stemming is neither used in roadway excavation nor mining stopping in the Kaiyang phosphate mine even though it has been demonstrated to be important in rock fragmentation. One of the main reasons is that the work of borehole stemming increases the duration of blasting operation. Therefore, to optimize the current blasting scheme, the contour boreholes are stemmed with wet sand because it is easy to get in the construction site.

The numerical results of rock damage in five sections are shown in Fig. 18. The overbreak extents in Section-1 to Section-5 were 20.03, 28.77, 34.56, 43.61 and 30.90 cm in sequence, and the differences between them and those in Fig. 12 were −4.1, 11.32, 5.2, 10.26, and −2.13 cm, respectively. The extents of underbreak induced by stemmed blastholes are smaller than those without hole stemming, indicating that stemming blasting exhibits higher efficiency in enhancing the useful explosion energy applied to the peripheral rock. In addition, the distributions of overbreak and underbreak are in good consistency with those in Fig. 12. It's worth noting that when the contour blastholes were stemming, the rock mass in the region where blastholes were not stemmed was fractured, and the overbreak was significantly controlled. Thus, in practical blasting operation, borehole stemming is suggested because it is extremely important to slow down the rate of the explosion wave although it takes a little longer time.

5.6 Limitations of the study

Although the simplified 3D model has been developed to simulate the blast-induced overbreak and underbreak in a deep underground roadway, this model can be used to investigate the influence of geological factors and blasting factors on rock damage, as well as predict the extents of

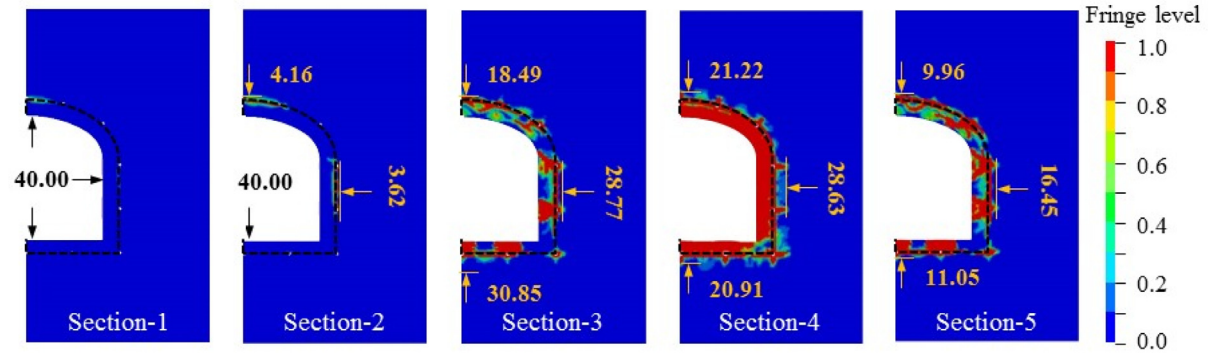

(a)

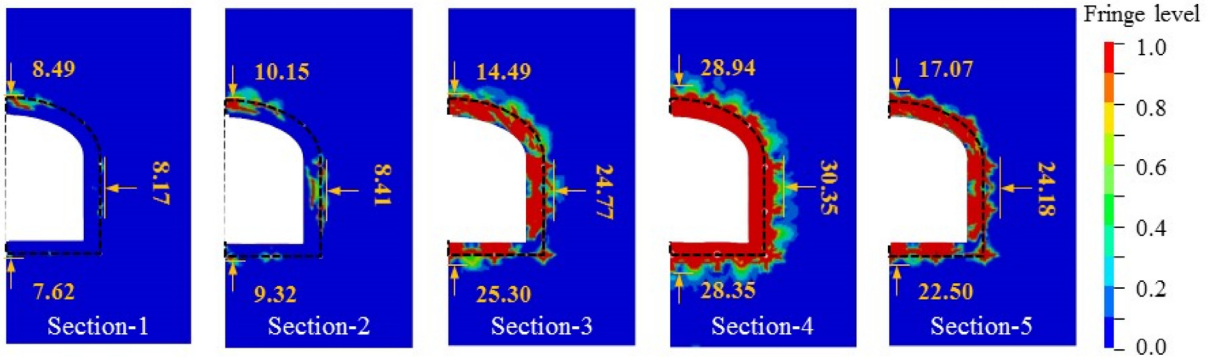

(b)

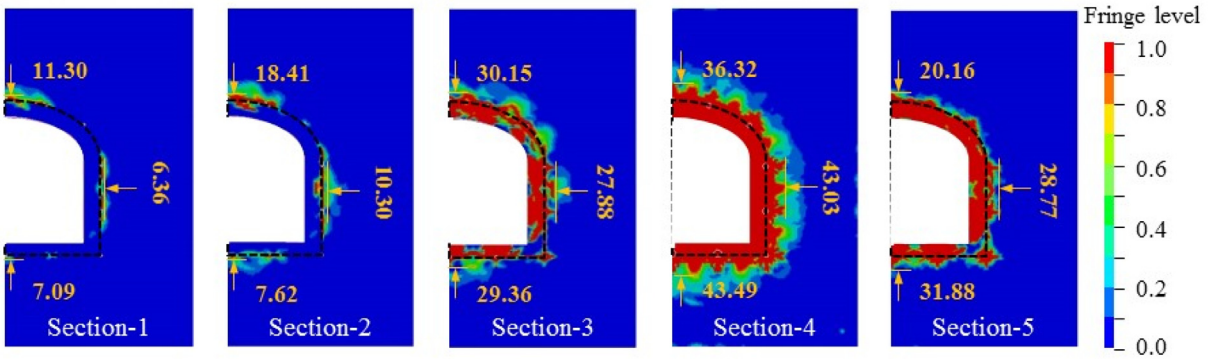

(c)

Fig. 17. Numerical results of blast-induced damage of rock within various decoupled coefficients. (a) $\zeta = 3.0$, (b) $\zeta = 2.5$, (c) $\zeta = 2.0$ (Unit: cm).

the overbreak and underbreak under specific engineering conditions. The reliability of simulation results still needs to be further improved considering the rock discontinuities and the degradation of rock properties.

The presence of discontinuities such as joints in the rock mass significantly affects the evolution of rock damage related to blasting excavation. Moreover, in practice, the rock mass near roadway face has been damaged due to the dynamic impact of previous blasting round, resulting in the degradation of rock physical and mechanical properties. The foregoing factors are the main reasons for the discrepancies between the simulation and field measurement results. Therefore, in future work, the existing natural joints in rock mass and properties degradation will be considered to improve the accuracy of the numerical model.

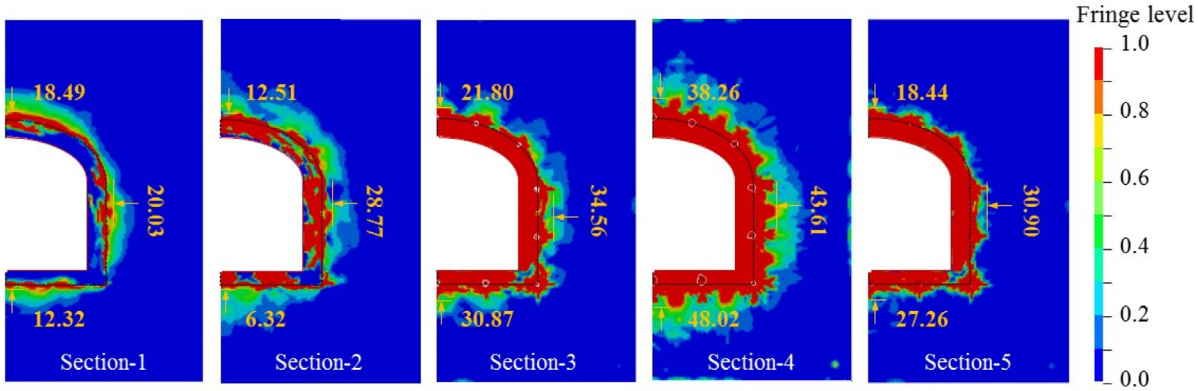

Fig. 18. The numerical result of roadway blasting excavation with sand stemming (Unit: cm).

6 Conclusion

In this study, one of the deep development roadways in the Kaiyang phosphate mine was selected as engineering background, the Focus^S 150 laser scanner was employed to scan the post-blast roadway contour surface, and the extent of the overbreak and underbreak was analyzed using a professional processing software. Moreover, a simplified 3D numerical model was developed, and it was validated based on one of the testing results. The blasting parameters including hole spacing, charge concentration, decoupled coefficient and stemming as well as in situ stress condition were considered for reducing the overbreak and underbreak. In summary, the following detailed conclusions are drawn:

(1) The field measurement results indicated that owing to the high stress concentration generated by in situ stress redistribution and blasting load, the extent of overbreak in the roadway crown was usually larger than that in sidewall. In addition, underbreak was more likely to appear in the corner at the bottom of the roadway, because the shear stress induced by dynamic stress concentration and the tensile stress induced by blasting wave were below the rock mass strength.

(2) A comparison of the extents of the overbreak and underbreak from the numerical model and field measurement indicates that the proposed simplified model of contour blasting is reliable and of great importance to taking a further insight into the evolution of the overbreak and underbreak.

(3) The extent of overbreak at roadway sidewall increased with the lateral pressure coefficient. In contrast, the overbreak at roadway roof gradually decreased. Moreover, the in situ stresses exceeding 30 MPa restrained the evolution of rock damage, implying that the overbreak could be well controlled under high in situ stress condition. The overbreak extent increased with the in situ stress as it was less than 30 MPa.

(4) A decrease in hole spacing resulted in a smoother excavation surface, and the underbreak exhibited a decreased tendency along with the decreased hole spacing. $S = 0.70$ m was suggested for contour hole spacing at a burden of 0.40 m. Furthermore, $\beta = 0.9$ was a proper choice which resulted in a minimum extent of the overbreak and underbreak. Correspondingly, $\zeta = 2.5$ was recommended in the practical blasting operation. Stemming exhibited a significant influence on the extent blast-induced rock damage because of the enhancement of explosive energy utilization.

Declaration of Competing Interest

The authors declare that they have no known competing financial interests or personal relationships that could have appeared to influence the work reported in this paper.

Acknowledgement

This study was jointly supported by the National Natural Science Foundation of China (Grant Nos. 11772357 and 12072376) and the Fundamental Research Funds for the Central Universities of Central South University (Grant No. 2021XQLH053).

References

Borrvall, T. (2011). The RHT concrete model in LS-DYNA. 8th European LS-DYNA conference. Strasbourg, France.

Chakraborty, A. K., Jethwa, J. L., & Paithankar, A. G. (1994). Assessing the effects of joint orientation and rock mass quality on fragmentation and overbreak in tunnel blasting. *Tunnelling and Underground Space Technology, 9*(4), 471–482.

Chen, J. H., Qiu, W. G., Zhao, X. W., Rai, P., Ai, X. F., & Wang, H. L. (2021). Experimental and numerical investigation on overbreak control considering the influence of initial support in tunnels. *Tunnelling and Underground Space Technology, 115*, 104017.

Cheng, R. S., Chen, W. S., Hao, H., & Li, J. D. (2021). A state-of-the-art review of road tunnel subjected to blast loads. *Tunnelling and Underground Space Technology, 112*, 103911.

Cheng, R. S., Zhou, Z. L., Chen, W. S., & Hao, H. (2022). Effects of axial air deck on blast-induced ground vibration. *Rock Mechanics and Rock Engineering, 55*(2), 1037–1053.

Dey, K., & Murthy, V. M. S. R. (2012). Prediction of blast-induced overbreak from uncontrolled burn-cut blasting in tunnels driven through medium rock class. *Tunnelling and Underground Space Technology, 28*, 49–56.

Foderà, G. M., Voza, A., Barovero, G., Tinti, F., & Boldini, D. (2020). Factors influencing overbreak volumes in drill-and-blast tunnel excavation. A statistical analysis applied to the case study of the Brenner Base Tunnel – BBT. *Tunnelling and Underground Space Technology, 105*, 103475.

Ganesan, G., & Mishra, A. K. (2021). Assessment of drilling inaccuracy and delineation of constructional and geological overbreak. *Tunnelling and Underground Space Technology, 108*, 103730.

Gong, F. Q., Li, X. B., & Zhang, W. (2008). Over-excavation forecast of underground opening by using Bayes discriminant analysis method. *Journal of Central South University of Technology, 15*(4), 498–502.

Hagan, T. (1982). *Controlling blast-induced cracking around large caverns*. Aachen, Germany: ISRM International Symposium.

Han, H., Fukuda, D., Liu, H., Fathi Salmi, E., Sellers, E., Liu, T., & Chan, A. (2020). FDEM simulation of rock damage evolution induced by contour blasting in the bench of tunnel at deep depth. *Tunnelling and Underground Space Technology, 103*, 103495.

Holmberg, R. (1979). Design of tunnel perimeter blasthole patterns to prevent rock damage. In *Proceedings of the 2nd International Symposium Tunneling*. London, England.

Hustrulid, W., & Johnson, J. (2008). A gas pressure-based drift round blast design methodology. In *5th International Conference & Exhibition on Mass Mining*. Lulea, Sweden.

Ibarra, J. A., Maerz, N. H., & Franklin, J. A. (1996). Overbreak and underbreak in underground openings Part 2: Causes and implications. *Geotechnical & Geological Engineering, 14*(4), 325–340.

Iverson, S., Hustrulid, W., & Johnson, J. (2013). *A New Perimeter Control Blast Design Concept for Underground Metallnonmetal Drifting Applications*. Pittsburgh: CreateSpace Independent Publishing Platform.

Jang, H., & Topal, E. (2013). Optimizing overbreak prediction based on geological parameters comparing multiple regression analysis and artificial neural network. *Tunnelling and Underground Space Technology, 38*, 161–169.

Kim, Y., Kim, H., Yoo, J. J. E., & Blasting. (2003). A study on the drilling methods to reduce overbreak in tunnel blasting. *Explosives and Blasting, 21*(2), 1–13.

Kim, Y., & Moon, H.-K. (2013). Application of the guideline for overbreak control in granitic rock masses in Korean tunnels. *Tunnelling and Underground Space Technology, 35*, 67–77.

Koopialipoor, M., Jahed Armaghani, D., Haghighi, M., & Ghaleini, E. N. (2019). A neuro-genetic predictive model to approximate overbreak induced by drilling and blasting operation in tunnels. *Bulletin of Engineering Geology and the Environment, 78*(2), 981–990.

Li, P. P., Qiu, W. G., Cheng, Y. J., & Lu, F. (2021). Application of 3D Laser Scanning in Underground Station Cavity Clusters. *Advances in Civil Engineering, 2021*, 8896363.

Liu, K., Yang, J., Li, X., Hao, H., Li, Q., Liu, Z., & Wang, C. (2018). Study on the long-hole raising technique using one blast based on vertical crater retreat multiple deck shots. *International Journal of Rock Mechanics and Mining Sciences, 109*, 52–67.

Liu, K. W., Li, X. D., Hao, H., Li, X. B., Sha, Y. Y., Wang, W. H., & Liu, X. L. (2019). Study on the raising technique using one blast based on the combination of long-hole presplitting and vertical crater retreat multiple-deck shots. *International Journal of Rock Mechanics and Mining Sciences, 113*, 41–58.

Lu, W. B., Yang, J. H., Yan, P., Chen, M., Zhou, C. B., Luo, Y., & Jin, L. (2012). Dynamic response of rock mass induced by the transient release of in-situ stress. *International Journal of Rock Mechanics and Mining Sciences, 53*, 129–141.

Mahtab, M. A., Rossler, K., Kalamaras, G. S., & Grasso, P. (1997). Assessment of geological overbreak for tunnel design and contractual claims. *International Journal of Rock Mechanics and Mining Sciences, 34*(3–4), 185.

Mohammadi, M., Hossaini, M. F., Mirzapour, B., & Hajiantilaki, N. (2015). Use of fuzzy set theory for minimizing overbreak in underground blasting operations – A case study of Alborz Tunnel, Iran. *International Journal of Mining Science and Technology, 25*(3), 439–445.

Mottahedi, A., Sereshki, F., & Ataei, M. (2018). Overbreak prediction in underground excavations using hybrid ANFIS-PSO model. *Tunnelling and Underground Space Technology, 80*, 1–9.

Murthy, V., Dey, K., & Raitani, R. (2003). Prediction of overbreak in underground tunnel blasting a case study. *Journal of Canadian Tunneling Canadien*, 109–115.

Pal, S., & Shahri, V. (2014). Geological overbreak: A viewpoint of storage cavern excavation. *Journal of Rock Mechanics & Tunnelling Technology, 20*(2), 121–129.

Read, R. S. (2004). 20 years of excavation response studies at AECL's Underground Research Laboratory. *International Journal of Rock Mechanics and Mining Sciences, 41*(8), 1251–1275.

Riedel, W., Thoma, K., Hiermaier, S., & Schmolinske, E. (1999). Penetration of reinforced concrete by BETA-B-500 numerical analysis using a new macroscopic concrete model for hydrocodes. In *9th International Symposium, Interaction of the Effects of Munitions with Structures*. Berlin, Germany.

Rustan, A. P. (1998). Micro-sequential contour blasting—how does it influence the surrounding rock mass? *Engineering Geology, 49*(3–4), 303–313.

Saiang, D. (2008). *Behaviour of blast-induced damaged zone around underground excavations in hard rock mass* [Doctoral dissertation, Luleå University of Technology, Sweden].

Singh, S. P., & Xavier, P. (2005). Causes, impact and control of overbreak in underground excavations. *Tunnelling and Underground Space Technology, 20*(1), 63–71.

Verma, H. K., Samadhiya, N. K., Singh, M., Goel, R. K., & Singh, P. K. (2018). Blast induced rock mass damage around tunnels. *Tunnelling and Underground Space Technology, 71*, 149–158.

Wang, M. N., Zhao, S. G., Tong, J. J., Wang, Z. L., Yao, M., Li, J. W., & Yi, W. H. (2021). Intelligent classification model of surrounding rock of tunnel using drilling and blasting method. *Underground Space, 6*(5), 539–550.

Warneke, J., Dwyer, J., & Orr, T. (2007). Use of a 3-D scanning laser to quantify drift geometry and overbreak due to blast damage in underground manned entries. In *1st Canada-US Rock Mechanics Symposium*. Vancouver, Canada.

Widodo, S., Anwar, H., & Syafitri, N. A. (2019). Comparative analysis of ANFO and emulsion application on overbreak and underbreak at blasting development activity in underground Deep Mill Level Zone (DMLZ) PT Freeport Indonesia. *IOP Conference Series: Earth and Environmental Science, 279*(1), 012001.

Xie, L. X., Zhang, Q. B., Gu, J. C., Lu, W. B., Yang, S. Q., Jing, H. W., & Wang, Z. L. (2019). Damage evolution mechanism in production blasting excavation under different stress fields. *Simulation Modelling Practice and Theory, 97*, 101969.

Yi, C. P., Johansson, D., & Greberg, J. (2018). Effects of in-situ stresses on the fracturing of rock by blasting. *Computers and Geotechnics, 104*, 321–330.

Yi, C. P., Nordlund, E., Zhang, P., Warema, S., & Shirzadegan, S. (2021). Numerical modeling for a simulated rockburst experiment using LS-DYNA. *Underground Space, 6*(2), 153–162.

Yi, C. P., Sjöberg, J., Johansson, D., & Petropoulos, N. (2017). A numerical study of the impact of short delays on rock fragmentation. *International Journal of Rock Mechanics and Mining Sciences, 100*, 250–254.

Zhang, Z. X., Hou, D. F., Guo, Z. R., & He, Z. W. (2020). Laboratory experiment of stemming impact on rock fragmentation by a high explosive. *Tunnelling and Underground Space Technology, 97*, 103257.

Zhang, Z. X., Qiao, Y., Chi, L. Y., & Hou, D. F. (2021). Experimental study of rock fragmentation under different stemming conditions in model blasting. *International Journal of Rock Mechanics and Mining Sciences, 143*, 104797.

Zhu, H. H., Yan, J. X., & Liang, W. H. (2019). Challenges and development prospects of ultra-long and ultra-deep mountain tunnels. *Engineering, 5*(3), 384–392.